Applied Catalysis B: Environmental 320 (2023) 121961

Contents lists available at ScienceDirect

Applied Catalysis B: Environmental

journal homepage: www.elsevier.com/locate/apcatb

Constructing hollow porous Pd/H-TiO_2 photocatalyst for highly selective photocatalytic oxidation of methane to methanol with O_2

Xibo Zhang [1], Yaqin Wang [1], Kuan Chang, Shuangli Yang, Huijie Liu, Qian Chen, Zhaoxiong Xie, Qin Kuang *

State Key Laboratory of Physical Chemistry of Solid Surfaces, Collaborative Innovation Center of Chemistry for Energy Materials, and Department of Chemistry, College of Chemistry and Chemical Engineering, Xiamen University, Xiamen 361005, China

ARTICLE INFO

Keywords:
Photocatalysis
Methane oxidation
TiO_2
Methanol

ABSTRACT

The partial oxidation of methane to methanol with O_2 is an attractive catalytic reaction, but the catalysts still face great challenges in terms of activity and selective oxidation, especially how to avoid overoxidation. Herein, Pd/H-TiO_2 with a unique hollow porous nanocage structure was prepared for selective photooxidation of methane into methanol by O_2 under mild conditions. The as-obtained Pd/H-TiO_2 exhibited a high methanol production rate of 4.5 mmol/g/h with selectivity reaching up to 70 % under optimized conditions, exceeding most reported values. The mechanism study indicated that •OH radicals, produced by photogenerated holes, played an important role in the activation of methane into $•CH_3$ species, and the latter was further oxidized into methanol by $•O_2$ radicals formed by photogenerated electrons. The strong metal-support interaction and unique porous hollow structure also effectively enhanced the catalytic activity. These new insights provide us guidance for the design of high-performance photocatalysts for selective photocatalytic oxidation of methane.

1. Introduction

Methanol is an important liquid fuel and feedstock for the manufacture of olefins, aromatics, and other fine chemicals. And it also could replace fossil fuels as an alternative energy source in energy storage and ground transportation, leading to a feasible "methanol economy" [1–3]. However, large-scale transformation of methane into methanol is usually based on an energy-intensive indirect conversion process *via* firstly producing synthesis gas (> 700 °C) under high temperatures and pressures [4–7]. Therefore, direct selective oxidation of methane to methanol under mild conditions is very attractive, thereby called by the "Holy Grail" reaction[6,8–13].

Among processes, photocatalysis may easily activate the first C–H bond in methane, thereby converting methane into methanol at low temperatures or even room temperature [14–21]. However, the grand challenge of photocatalysis is to achieve high activity and selectivity of methanol at the same time [22–24]. Although high yields of liquid products can be obtained, avoiding the formation of by-product formaldehyde (HCHO) and methyl peroxide (CH_3OOH) is still quite difficult, leading to the poor selectivity of methanol [25]. Additionally, H_2O_2 is used as an oxidant in most photocatalytic systems, resulting in the high cost and low economic value [26]. In this regard, molecular oxygen (O_2) is more ideal for the oxidation of methane but much more difficult to activate CH_4 than H_2O_2 [27,28]. Therefore, the photocatalytic oxidation of methane using O_2 as the oxidant to achieve a high yield and methanol selectivity simultaneously is still challenging to date.

TiO_2 is a classic semiconductor photocatalyst that attracted extensive attention in the photooxidation of methane [29,30]. Various strategies have so far been proposed to improve the yield and selectivity of methanol and achieve desired catalysis efficiency, such as loading metal nanoparticles (NPs) as co-catalysts and engineering surface structure over TiO_2 based catalysts [16,25,31]. Thereinto, the hollowing structure has attracted intense attention in TiO_2 based photocatalysis since it can improve light scattering, reduce charge migration distance, and decline direct charge separation to endow photocatalysts with excellent photocatalytic performance [32,33]. In this work, hollowing strategy and loading metal co-catalysts are combined to synthesize high-performance TiO_2 based photocatalyst. Specifically, hollow porous TiO_2 (H-TiO_2) nanocages were prepared through the pyrolysis of Ti-based MOF (MIL-125-NH_2) and Pd NPs as co-catalysts were loaded onto H-TiO_2 by a

* Corresponding author.
E-mail address: qkuang@xmu.edu.cn (Q. Kuang).
[1] These authors equally contribute to the work.

https://doi.org/10.1016/j.apcatb.2022.121961
Received 28 June 2022; Received in revised form 2 September 2022; Accepted 5 September 2022
Available online 12 September 2022

photochemical route. The resulting Pd/H-TiO_2 showed excellent performance toward photocatalysis of methane oxidation with molecular oxygen. Under the optimized condition (3 MPa), the methanol production rate over Pd/H-TiO_2 reached 4.5 mmol/g/h and selectivity attained 70 %, superior to most reported values. The mechanism study demonstrated that the unique hollow structure and strong metal-support interaction of Pd/H-TiO_2 synergistically promoted the photocatalytic performance.

2. Experimental

2.1. Chemicals and materials

Chloroauric acid ($HAuCl_4 \cdot 4H_2O$, 99.9 %), Pd chloride (II) ($PdCl_2$, 99.9 %), chloroplatinic acid ($H_2PtCl_6 \cdot 6H_2O$), silver nitrate ($AgNO_3$ 99.8 %), N, N-dimethylformamide (DMF, 99.5 %) and methanol (99.5 %) were purchased from Sinopharm Chemical Reagent Co., Ltd. Titanium (IV) isopropoxide ($C_{12}H_{28}O_4Ti$, 99 %), polyvinyl pyrrolidone (PVP, K30), and 2-aminoterephthalic acid (H_2ATA, 98 %) were purchased from Energy Chemical. All chemicals were analytical graded and used without further purification.

2.2. Material synthesis

2.2.1. Synthesis of MIL-125-NH$_2$

First, 75 mg H_2ATA was dispersed in a mixture of 7 mL DMF and 3 mL methanol. Then, 75 μL $C_{12}H_{28}O_4Ti$ was added to the reaction mixture and sonicated for 5 min. Next, the above mixture was transferred into a 25 mL Teflon-lined stainless-steel autoclave and heated at 150 °C for 24 h. The obtained product was centrifuged, washed several times with ethanol, and finally dried in an oven overnight at 60 °C.

2.2.2. Synthesis of H-TiO$_2$

500 mg of MIL-125-NH_2 precursor was placed in a porcelain boat and calcined by a muffle furnace with the ramp of 1 °C/min to 500 °C for 4 h.

2.2.3. Syntheses of metal (Pd, Pt, Au, Ag)/H-TiO$_2$ and Pd/C-TiO$_2$

2.2.3.1. Pd/H-TiO$_2$. 30 mg prepared H-TiO_2 and 20 mg PVP were added to a mixed solution of 30 mL of H_2O and 1 mL of methanol. And 200 μL H_2PdCl_4 (1 mg_{pd}/mL) was added into the above solution. The mixture was irradiated by a 300 W Xe lamp equipped with a UV filter ($\lambda < 400$ nm) for 2 h under stirring. The sample was centrifuged, washed with ethanol for several times, and finally dried in an oven overnight at 60 °C.

2.2.3.2. Metal (Pt, Au, Ag)/H-TiO$_2$. The H_2PdCl_4 was changed into $H_2PtCl_6 \cdot 6H_2O$, $HAuCl_4 \cdot 4H_2O$, and $AgNO_3$ with the same metal content. The other steps were the same as Pd/H-TiO_2.

2.2.3.3. Pd/C-TiO$_2$. H-TiO_2 was changed into commercial TiO_2 (anatase crystal structure). The other steps were the same as Pd/H-TiO_2.

2.2.4. Synthesis of Pd + H-TiO$_2$

0.2 mg Pd black and 30 mL H-TiO_2 were dispersed into 30 mL H_2O. And the mixed solution was stirred for 4 h. The sample was centrifuged and washed with ethanol for several times and the resulting powder was dried in an oven overnight at 60 °C.

2.3. Characterization of samples

The morphology and structure of as-prepared catalysts were measured by scanning electron microscope (SEM, Hitachi S4800). High-angle annular dark-field scanning transmission electron microscopy (HAADF-STEM) and energy dispersive X-ray spectroscopy (EDS) mapping were measured on transmission electron microscope (TEM, Tecnai F30) with an accelerating voltage of 300 kV. The crystal phase of as-prepared products was determined by powder X-ray diffraction (XRD, Rigaku Ultima IV X-ray diffractometer) with Cu Kα radiation (λ = 1.54056 Å). The precise contents of metal elements in samples were determined by inductively coupled plasma-mass spectrometry (ICP-MS, Agilent 7700x). Electron paramagnetic resonance (EPR) spectra were obtained by using Bruker X-band A200. X-ray photoelectron spectroscopy (XPS) was measured on the PHI Quantum-2000 system, and a monochromatic aluminum anode with Kα radiation (1486.6 eV) was used as the X-ray source. All XPS spectra were calibrated with the C1s peak at 284.8 eV as the internal standard. Solid UV–vis absorption spectra were measured on Carry 5000. *In situ* diffuse reflectance infrared Fourier transform spectroscopy (DRIFTS) was tested on an infrared spectrometer (NICOLET 6700), in which a 300 W Xe lamp (equipped with 420 nm band pass filter) was employed as light source.

2.4. Catalytic tests

The performances of samples on photocatalytic oxidation of methane were evaluated in a commercial evaluation system (CEL-HPR100T+, Beijing China Education Au-Light Co., Ltd). First, 10 mg catalyst was dispersed in a quartz lining filled with 60 mL H_2O and transferred into the bottom of a stainless-steel reactor with a quartz window (diameter: 3.5 cm). After being sealed, the reactor was flushed several times to remove the air and then filled with 2 MPa CH_4/O_2 mixed gas (CH_4:98 %, O_2:2 %). Next, the reactor was irradiated by a 300 W Xe lamp (PLS-SXE300D, Perfectlight.cn.). The final products were detected by gas chromatography (SHIMADXU GC-2014C) equipped with a flame ionization detector and thermal conductivity detector. The liquid phase product was detected by 500 M NMR (AVANCE III HD 500 MHz), and dimethyl Sulfoxide (DMSO) diluted 10,000 times was added as an internal standard. For detecting HCHO, the reagent aqueous solution was prepared by dissolving 15 g ammonium acetate, 0.3 mL of acetic acid, and 0.2 mL of pentane-2,4-dione in 100 mL water. Then, 0.5 mL of liquid product was mixed with 1.0 mL of water and 0.5 mL of reagent solution. The mixed solution was maintained at room temperature for 3 h and measured the absorption intensity at 413 nm by UV–vis absorption spectroscopy.

2.5. In situ DRIFT

The catalyst powder was placed in the DRIFTS cell. He (99.9995 %) was used to purge the cell for 30 min. After that, the CH_4/O_2 mixed gas (CH_4:98 %, O_2:2 %) was introduced through a glass tube filled with H_2O for 30 min. Light was then introduced through the window of the cell and the data was collected every 10 min.

2.6. In situ EPR

5 mg Pd/H-TiO_2 was dispersed in 5 mL aqueous solution. And CH_4/O_2 gas mixture was bubbled into the above solution for 20 min. Take 200 μL of the mixture and add 40 μL of 5,5-dimethyl-1-pyrroline N-oxide (DMPO). Then, Xe lamp irradiation was introduced and detected the signal at 5 min, 10 min and 15 min. For detecting $\bullet O_2^-$, the Pd/H-TiO_2 was dispersed in 5 mL of methanol solution. And O_2 gas was bubbled into the above solution for 20 min. Other steps were the same as above to detect $\bullet OH^-$.

3. Results and discussion

3.1. Catalyst characterizations

The synthesis process of Pd/H-TiO_2 is schematically illustrated in Fig. 1**a**. First, MIL-125-NH_2 precursors shaped as square bricks with side length of about 800 nm and thickness of about 300 nm were synthesized

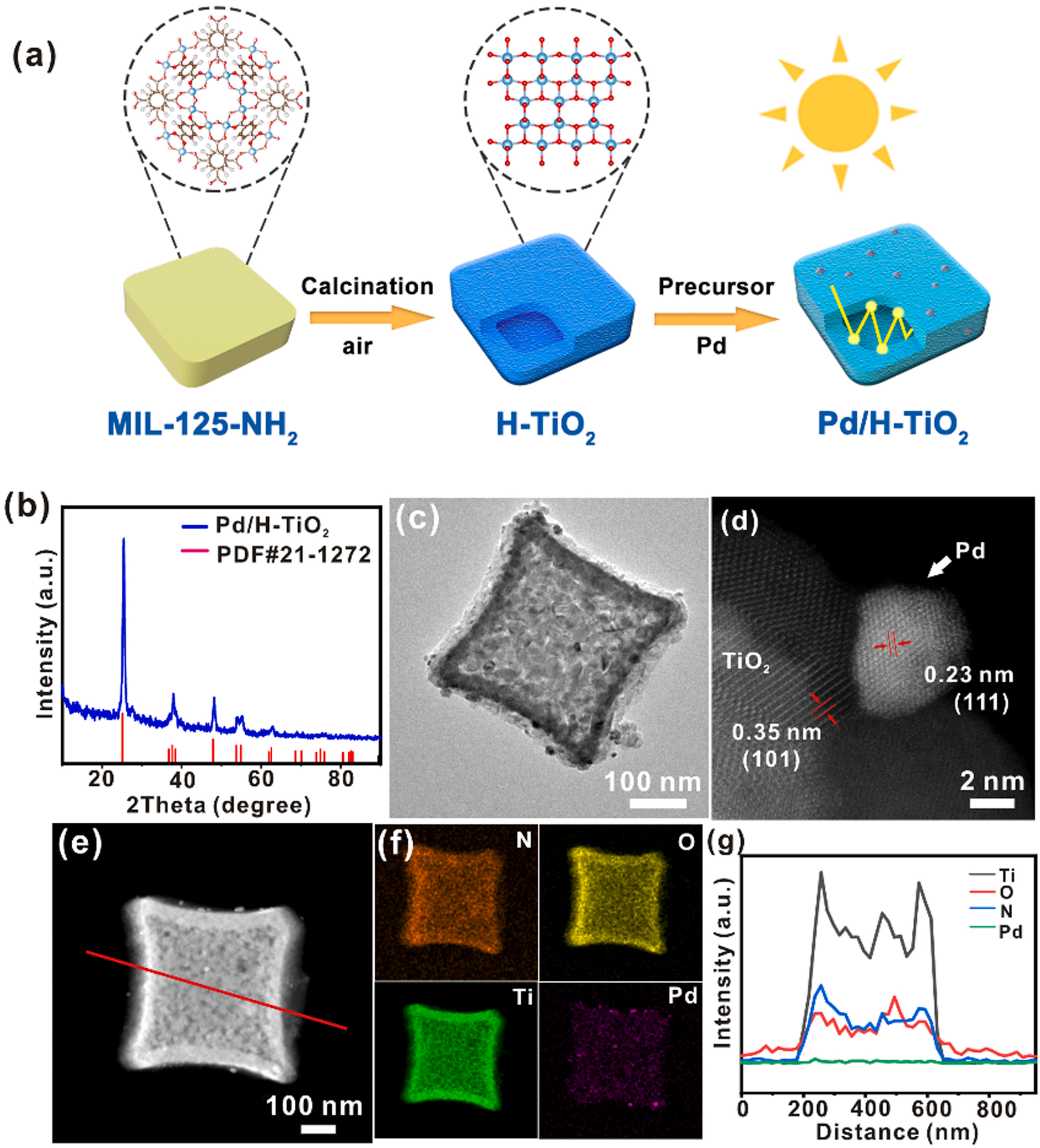

Fig. 1. (a) Scheme illustrating the synthesis of Pd/H-TiO_2 with the architecture of porous nanocage. (b) XRD pattern of Pd/H-TiO_2, (c) low-magnification TEM image of individual Pd/H-TiO_2 nanocage and its local HRTEM image, (d–f) HAADF-STEM image and corresponding EDS maps of individual Pd/H-TiO_2 nanocage, (g) EDS elemental line profiles of Pd/H-TiO_2 along the red line in (e).

by a hydrothermal route (Fig. S1). Next, MIL-125-NH_2 precursors were calcined in the muffle furnace at 500 °C for 4 h to form a hollow TiO_2 structure (H-TiO_2). As shown in Fig. S2**,** the products after calcination maintained the morphology of square brick. However, TEM observation revealed a transformation into a hollow structure with a wall thickness of 40–50 nm **(**Fig. S3**)**. The adsorption/desorption isotherm measurement revealed that H-TiO_2 exhibited obviously mesoporous characteristics and its specific surface area reached 16 m^2 g^{-1} **(**Fig. S4**)**. Finally, Pd NPs were loaded onto H-TiO_2 through a facile photochemically reduction route to form Pd/H-TiO_2 **(**Fig. S5**)**.

The powder XRD pattern of the as-synthesized Pd/H-TiO_2 is displayed in Fig. 1**b.** Only peaks of anatase TiO_2 were observed due to the low content of Pd, determined as only 0.52 wt% by ICP-MS. As revealed by TEM (Fig. 1**c**), some Pd NPs of 5–10 nm with deeper contrast randomly decorated the surface of hollow TiO_2 nanocages. The corresponding HRTEM image (Fig. 1**d)** further confirmed well-crystallized Pd

NPs and H-TiO_2 with very strong contact between both. A clear Pd/TiO_2 interface was observed, in which the lattice fringes of 0.35 nm and 0.23 nm corresponded to TiO_2 (101) plane and Pd (111) plane, respectively. Of note, HAADF-STEM image and corresponding EDS elemental maps of Pd/H-TiO_2 (Fig. 1**e–f**) revealed that N atoms from -NH_2 group were doped into the lattice of H-TiO_2 during pyrolysis of MIL-125-NH_2. The EDS elemental line profiles of Pd/H-TiO_2 further verified catalyst exhibiting a unique hollow structure (Fig. 1**g**). The solid UV–vis absorption spectra (Fig. S6) illustrated an absorption edge of H-TiO_2 around 416 nm, corresponding the band gap of 2.98 eV by the Tauc's plots [34]. After loading Pd nanoparticles, the band gap of Pd/H-TiO_2 decreases to 2.68 eV, indicating the formation of a metal-semiconductor heterojunction. Of note, the light absorption ability of the catalyst in the visible range was significantly enhanced after loading of H-TiO_2 with Pd NPs. Obviously, the enhanced light absorption would be beneficial to the improvement of photocatalytic performance.

3.2. Catalytic performances

The performance of Pd/H-TiO_2 toward the photocatalytic oxidation of methane in the presence of O_2 (2 %) was tested. For comparative purposes, Au/H-TiO_2, Pt/H-TiO_2, and Ag/H-TiO_2 with Au, Ag, and Pt NPs loaded onto H-TiO_2 were also synthesized by the same method and metal contents to severe as control catalysts (Fig. S7–8). The detailed properties of relevant catalysts are summarized in Table S1. As shown in Fig. 2**a**, the H-TiO_2 has the ability to convert methane into CO_2, CH_3OOH, HCHO, and CH_3OH. However, both the production rate (0.18 mmol/g/h) and selectivity (9.2%) of methanol were very low. By contrast, all M/H-TiO_2 (M = Au, Ag, Pd, and Pt) showed significantly improved activity and selectivity. Among M/H-TiO_2 catalysts, Pd/H-TiO_2 exhibited the best performance in converting CH_4 into methanol. The production rate of methanol over Pd/H-TiO_2 reached 2.4 mmol/g/h, a value 13-fold that of H-TiO_2. Also, the selectivity of methanol significantly increased from 9.2 % to 54.8 %. In our experiments, the concentration of methanol was determined by ^{1}H NMR spectroscopy and the concentration of HCHO in liquid products was measured by the acetylacetone color method (Fig. S9–11). The results also show that the M/TiO_2 heterostructure effectively enhanced the methane conversion rate. However, various metals played a distinct effect on product selectivity. For Au/H-TiO_2 and Ag/H-TiO_2, loading of Au and Ag NPs enhanced the yield of liquid products, but avoiding the formation of HCHO and CH_3OOH by-products was still challenging, thereby leading to the low methanol selectivity of 28.9 % and 24.6 %, respectively. Note that CH_3OOH can be obtained in the liquid products over Au/H-TiO_2 and Ag/H-TiO_2, different from Pt/H-TiO_2 and Pd/H-TiO_2. The reason for this may have to do with Pd and Pt NPs as co-catalysts, which exhibited a relatively higher activity to convert important intermediates of CH_3OOH into CH_3OH [35].

In order to explore the influence of metal deposition methods, other control catalysts were also prepared by physically mixing and H_2 reduction (denoted as Pd + H-TiO_2 and Pd/H-TiO_2(H_2), respectively). The HAADF-STEM images indicated no obvious Pd-TiO_2 interface in Pd + H-TiO_2, and Pd/H-TiO_2(H_2) showed smaller sized Pd NPs (Fig. S12). The methanol production rates over Pd + H-TiO_2 and Pd/H-TiO_2(H_2) were 0.42 mmol/g/h and 0.65 mmol/g/h, respectively, which were much lower than that of Pd/H-TiO_2 (Fig. 2**b**). In addition, for the Pd + H-TiO_2 and Pd/H-TiO_2(H_2), HCHO and CH_3OOH were the main liquid products, and methanol selectivity were only 17.8 % and 20.2 %, respectively. Thus, the difference in the interaction between Pd and H-TiO_2 caused by different deposition methods significantly affected the catalytic process. Commercial anatase TiO_2 with a low specific surface area (4.9 m^2 g^{-1}) was then used for comparison to explore the impact of H-TiO_2 hollow structure on photocatalytic performance (denoted as Pd/C-TiO_2, Fig. S12–13). The data revealed methanol production rate over

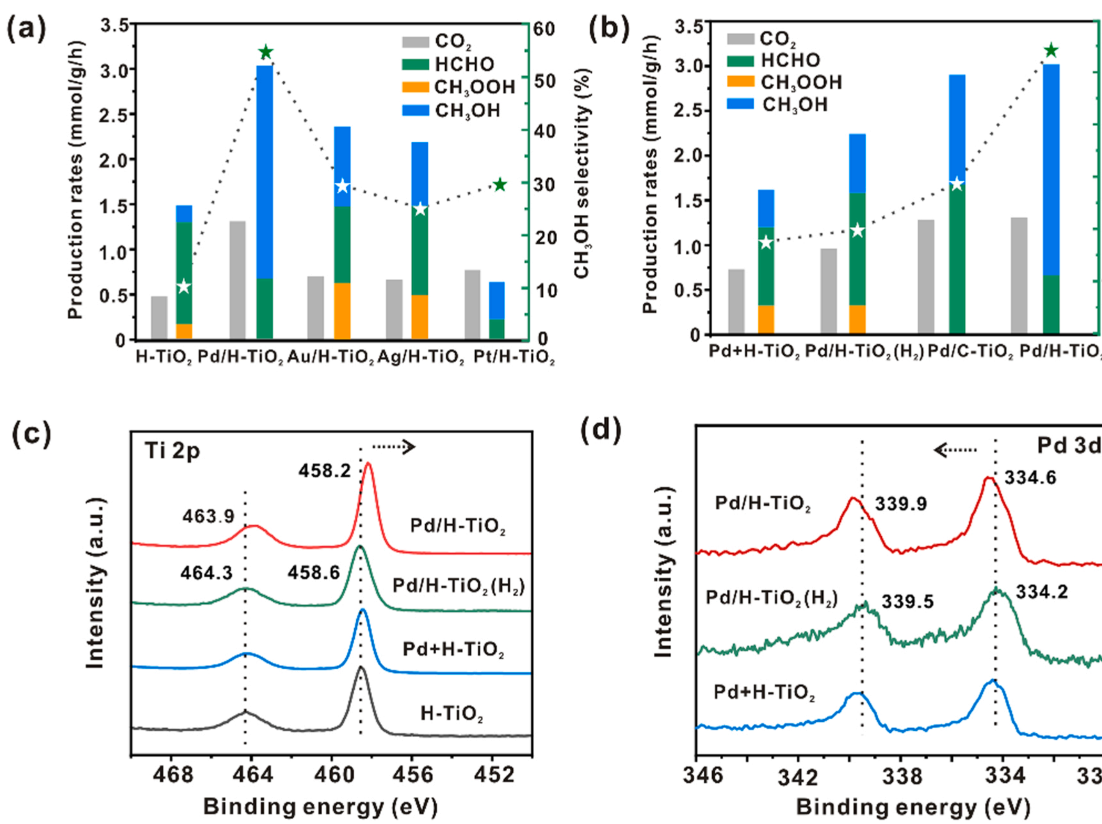

Fig. 2. Production rates obtained by the prepared catalysts: (a) H-TiO_2 and when loaded with different metals, (b) different metal deposition methods on various TiO_2 support. Reaction conditions: 10 mg cat., 60 mL water, 2 MPa, CH_4:O_2 50:1, 45 °C, and light source of 300 W Xe lamp, 350–780 nm and 1.0 W/cm^2. (c) Ti 2p high-resolution XPS spectra of related samples. (d) Pd 3d high-resolution XPS spectra of related samples.

Pd/C-TiO_2 reaching 1.2 mmol/g/h, a value only half that of Pd/H-TiO_2. Also, the methanol selectivity was estimated to 29.2 %, a value much lower than that of Pd/H-TiO_2 (54.8 %). Clearly, the unique porous hollow structure of H-TiO_2 induced better catalytic performance due to the porous hollow structure conducive to improving light scattering, reducing charge migration distance, and directing charge separation [33].

Based on the above results, it can be seen that the interaction between Pd and H-TiO_2 played a key role in promoting the photocatalytic activity and selectivity. To figure out the reasons, XPS analysis was conducted to explore the electronic structures of related catalysts. In the Ti 2p high-resolution XPS spectra, the peaks of Pd/H-TiO_2 shifted to lower binding energies (0.4 eV) when compared to H-TiO_2 (Fig. 2**c**). Similar phenomenon was also observed in the O1s high-resolution XPS spectra of Pd/H-TiO_2 (Fig. S14). However, the binding energies of Ti 2p and O1s in Pd + H-TiO_2 and Pd/H-TiO_2(H_2) were almost the same as those of H-TiO_2. In addition, the binding energies of Pd 3d in Pd/H-TiO_2 shifted to higher energies (0.4 eV) when compared to Pd + H-TiO_2 and Pd/H-TiO_2(H_2), indicating electrons transfer from Pd to H-TiO_2 (Fig. 2**d**). Therefore, Pd/H-TiO_2 possessed stronger metal-support interaction than Pd + H-TiO_2 and Pd/H-TiO_2(H_2), beneficial to the transfer of photogenerated electrons during photocatalysis. The EPR spectra of H-TiO_2, Pd/H-TiO_2 and Pd/H-TiO_2 (H_2) during reaction were tested. The results showed that the generation rate of active specie •OH was increased after loading Pd during reaction, but the photo-deposition method (Pd/H-TiO_2) was significantly better than that of H_2 reduction (Pd/H-TiO_2 (H_2)) due to stronger metal-support interaction (Fig. S15.). In addition, photoluminescence (PL) and photocurrent spectra were measured to study the separation of photogenerated charges and the results are shown in Fig. S16. The lower PL peak intensity of Pd/H-TiO_2

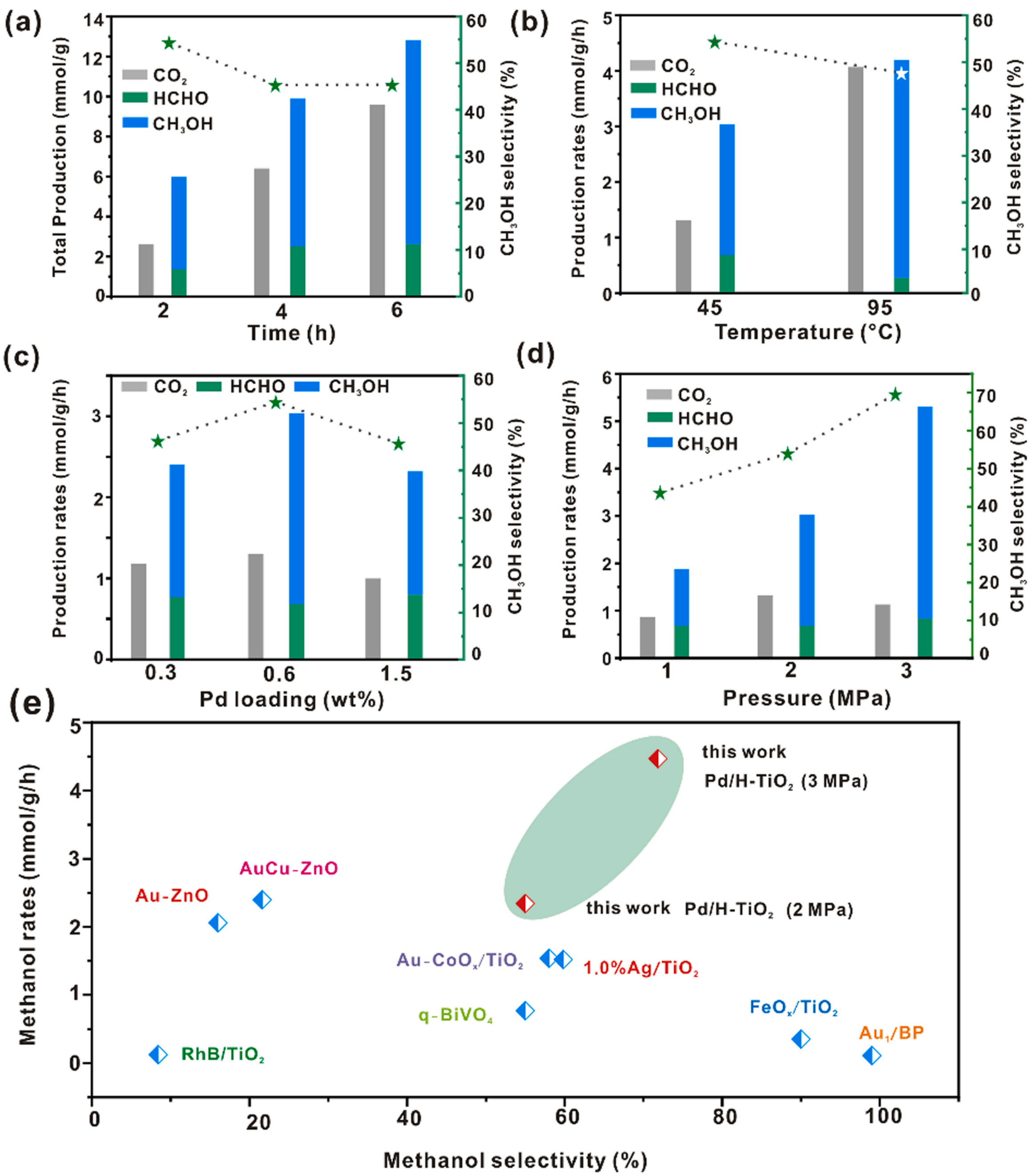

Fig. 3. (a) Dependence of methane oxidation over Pd/H-TiO_2 with irradiation time. (b–d) Production rates over Pd/H-TiO_2 at different temperatures, Pd loading amounts, and pressures. (e) Performance comparison of Pd/H-TiO_2 with other catalysts under similar conditions.

suggested that loading Pd particles helps to suppress recombination of photogenerated charges. In addition, Pd/H-TiO_2 also exhibited a higher photocurrent response compared with H-TiO_2, indicating faster and more efficient separation of photogenerated charges.

The catalytic performance of Pd/H-TiO_2 was further optimized under different conditions. To this end, catalytic tests were performed with different times (2, 4, and 6 h). As shown in Fig. 3**a**, the production of methanol increased with the irradiation time, while the selectivity decreased slightly. This was mainly attributed to the problem of the batch reaction system, where the produced methanol remained in the reactor and thus were easily oxidized further. Despite all this, the selectivity of methanol was still above 45 % after 6 h reaction. The rise in reaction temperature from 45 ℃ to 95 ℃ led to the enhanced production rate of methanol by 1.6-fold, while selectivity slightly dropped from 54.8 % to 47.5% (Fig. 3**b**). The above results revealed that increasing the reaction time and temperature can indeed promote the conversion of methane, but at the same time, it intensified the excessive oxidation of methanol to CO_2, resulting in unsatisfactory selectivity. The loading amount of Pd NPs in Pd/H-TiO_2 catalyst was also optimized, and the results showed a volcanic curve **(**Fig. 3**c)**. The catalytic performance of 0.6 wt% Pd/H-TiO_2 was better than those of 0.3 wt% and 1.5 wt% Pd/H-TiO_2 (Pd loading as feeding content). In addition, the catalytic performances were tested under different pressures from 1 MPa to 3 MPa (Fig. 3**d**).The production rate and selectivity of methanol increased obviously with pressure. Under 3 MPa, the production rate of methanol over Pd/H-TiO_2 reached 4.5 mmol/g/h and selectivity was up to 70 %. We also evaluated the catalytic performance over Pd/H-TiO_2 at different water amounts (20, 40, and 60 mL) (Fig. S17). The results show that the yield and selectivity of liquid products significantly increased with higher water amount. The results show that increasing water amount and pressure are effective methods to improve methanol yield and selectivity, possibly by increasing the solubility of methane. The TEM and XRD of used Pd/H-TiO_2 were also characterized in Fig. S18. The results show that the structure of catalyst was still maintained after the reaction, indicating that it has a good structure stability. To better evaluate the photocatalytic performance of Pd/H-TiO_2, the results were also compared with typical catalysts reported in the literature. In Table S2**,** even though some reported catalysts exhibited high selectivity of oxygenate, the selectivity to target product methanol was still low. Additionally, achieving a high production rate and high selectivity of methanol at the same time was rarely reported. In this regard, Pd/H-TiO_2 are far superior to most reported catalysts (Fig. 3**e**). The strong interaction between Pd NPs and H-TiO_2 coupled with the unique hollow porous structure synergistically promoted the partial photo-oxidation of methane to methanol.

3.3. Mechanism analysis

Since the photooxidation of methane involves various active species, obtaining a unified reaction pathway is difficult due to similarities between reaction intermediates. For example, intermediate hydroxyl radicals may directly react with methyl groups to form methanol or may act as reactive species to activate C-H in methane [35]. To gain a better understanding of the catalytic process, various blank experiments with different reactants were conducted and the data are gathered in Fig. S19. When the reactants were changed to O_2 and water, no product was observed, indicating that methanol did not originate from contaminants. Not only that, methanol cannot be produced from the reaction between CH_4 and H_2O, suggesting the crucial role of O_2 in promoting the conversion of methane to methanol [36,37].

To further explore the reaction mechanism, multiple monitoring technologies, including *in-situ* EPR, *ex situ*-XPS, and *in-situ* DRIFT were used to detect the reaction intermediates. *In-situ* EPR can effectively detect reactive oxygen species (ROS) during the photocatalytic process. The irradiation of the reaction aqueous solution dissolving CH_4 and O_2 in water generated obvious equidistant quartet signals, belonging to •OH radicals with intensity increasing with extending irradiation time (Fig. 4**a**). When the *in-situ* EPR measurement was performed in methanol aqueous solution dissolving O_2, signals assigned to superoxide anion (•O_2^-) were detected, and the intensity increased with the irradiation time (Fig. 4**b**). Thus, it can be deduced that •O_2^- and •OH were the two main ROS in photocatalytic methane oxidation.

Further trapping experiments were also performed to determine the roles of these radicals in the selective oxidation of CH_4. Here, para-quinone and salicylic acid were added into reaction solution as sacrificial agents of •O_2^- and •OH, respectively (Fig. 4**c**). As shown in Fig. 4**c,** methanol was no longer produced after the addition of para-quinone or salicylic acid. It can be seen that •O_2^- and •OH played an indispensable role in the reaction process. To illustrate the origin of oxygen in methanol, the isotope experiment ($^{18}O_2$) was performed. The results proved that oxygen in methanol was mainly derived from O_2 (Fig. S20). However, when •OH was trapped by salicylic acid (Fig. S21), methanol cannot be achieved anymore. That means that •OH play an important role to abstract H from methane to from •CH_3 [35]. Methanol was also not observed after trapping •O_2^-, indicating that •O_2^- mainly promoted •CH_3 radicals into methanol, which is consistent with isotope experiments.

Ex-situ XPS was carried out to analyze C species and metal valence of catalysts during reactions. Through deconvolution**,** it was found that O=C-O (287.3 eV), which was an important intermediate for the over-oxidation of methane to CO_2, rose significantly after illumination (Fig. 4**d**) [38]. Furthermore, large numbers of oxygen vacancies were generated on the surface of TiO_2 under illumination. Accordingly, the valence of Ti then decreased, consistent with the lower binding energy of Ti 2p in Fig. 4**e**. By contrast, the binding energy of Pd 3d did not change under illumination, suggesting Pd NPs in Pd/H-TiO_2 remained in the metallic state (Fig. S22).

In-situ DRIFT was also conducted to observe the reaction intermediates over Pd/H-TiO_2. As provided in Fig. S23, the intensities of CO_2 peaks at 2356 cm^{-1} and 2339 cm^{-1} significantly increased as a function of illumination time, directly proving the occurrence of photocatalytic methane conversion. In addition, a new band appeared at 2888 cm^{-1} under light illumination, assigned to the stretching vibration of the C—H bond of methoxy groups [25]. Meanwhile, overoxidation products were detected at 1721, 1615, and 1481 cm^{-1}, which are attributed to ν(CO) stretching of adsorbed CH_2O*, HCOO*, and $\delta(CH_2)$ of H_2COO* species, respectively [39].

Based on these results, the oxidation mechanism of methane to methanol over Pd/H-TiO_2 was extracted and schematically summarized in Fig. 4**g**. In this process, Pd/H-TiO_2 was first excited to generate electron-hole pairs under illumination (1). The H_2O was then oxidized by holes to produce •OH radicals (2), and O_2 was reduced by electrons to O_2^- (3). Next, •OH activated CH_4 to generate •CH_3 (4). Isotope experiments and trapping experiments proved that the oxygen in methanol was derived from O_2 not H_2O. Therefore, the main reaction pathway consisted of •CH_3 reacting with O_2^- to form CH_3OOH, which then was converted to methanol (5). In this way, Pd/H-TiO_2 simultaneously achieved high-yield and selective photocatalytic conversion of methane to methanol.

4. Conclusions

Hollow porous Pd/H-TiO_2 nanocages were obtained by pyrolysis of MIL-125-NH_2 followed by photodeposition. Under the optimized conditions, Pd/H-TiO_2 achieved a high methanol production rate of 4.5 mmol/g/h with selectivity as high as 70 %, exceeding most literature reports. The excellent performance was related to the unique hollow porous structure, suitable Pd co-catalyst, and strong interaction between Pd and TiO_2 constructed by photodeposition. Furthermore, a deeper understanding of the catalytic mechanism was obtained by *in-situ* ESR, *ex-situ* XPS, and *in-situ* DRIFT. The results showed •OH and •O_2^- as the main active species involved in the photocatalytic process. Among

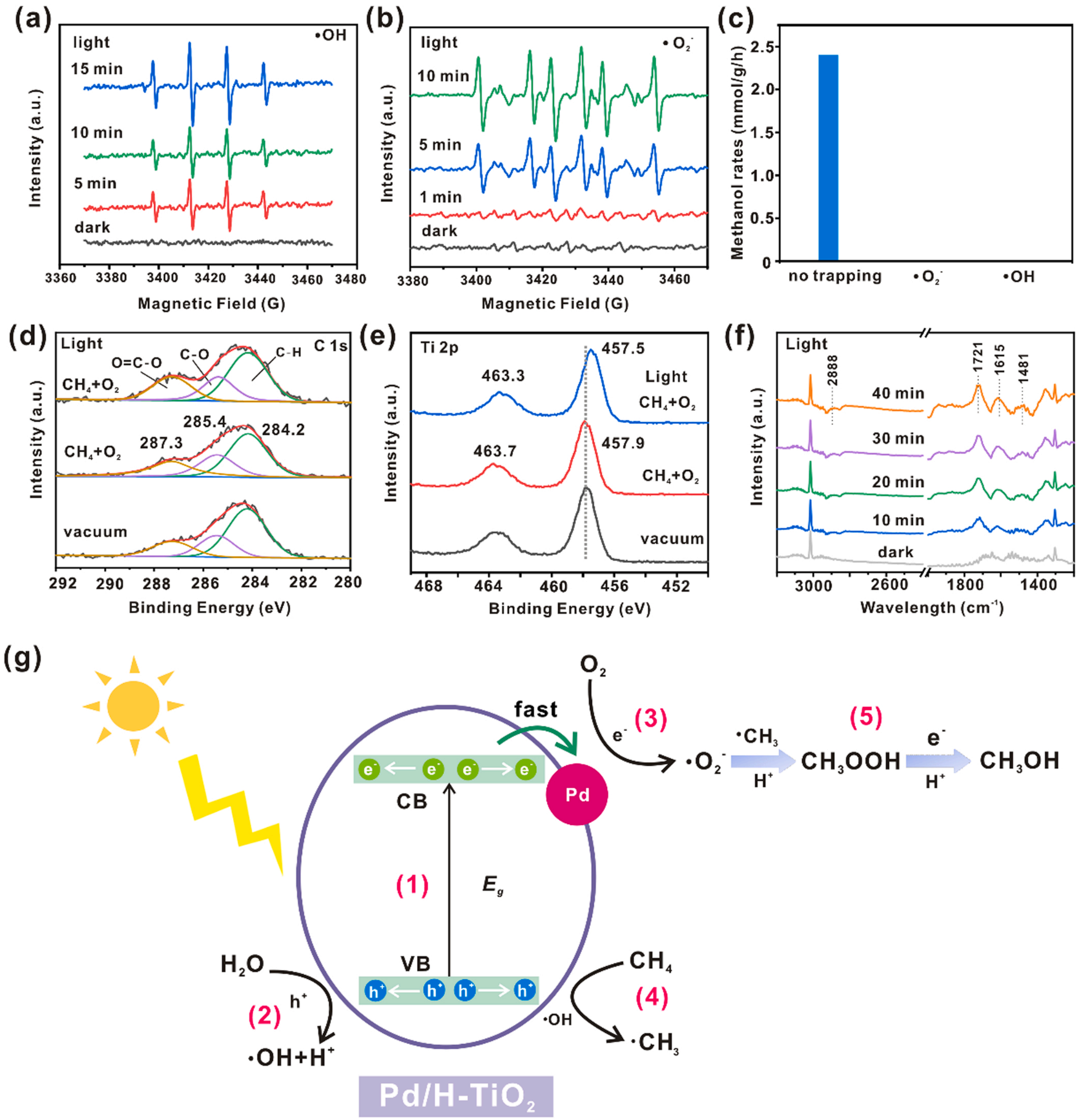

Fig. 4. *In-situ* EPR spectra of Pd/H-TiO_2 obtained by: (a) dissolving CH_4 and O_2 in water with different light illumination times, (b) dissolving O_2 in CH_3OH aqueous solution with different light illumination times. DMPO is used as the radical trapping agent. (c) Changes in products of CH_4 oxidation after the addition of scavengers para-quinone and salicylic acid in the reaction system for trapping $\bullet O_2^-$ and •OH, respectively. (d–e) *Ex-situ* XPS spectra of C 1s and Ti 2p of Pd/H-TiO_2 under vacuum, CH_4, and O_2 atmosphere and light irradiation. (f) *In-situ* DRIFT spectra of Pd/H-TiO_2. (g) The proposed catalytic mechanism for the oxidation of methane to methanol over Pd/H-TiO_2.

these, •OH played an important role in activating methane into $\bullet CH_3$, and $\bullet O_2^-$ showed a better performance in further converting $\bullet CH_3$ into methanol. In sum, new insights into the synthesis of photocatalysts and the mechanism of photooxidation of methane to methanol were provided, which might be useful for future synthesis of high-performance photocatalysts for photooxidation of methane to methanol.

CRediT authorship contribution statement

Xibo Zhang: Conceptualization, Methodology, Software, Data curation, Investigation, Writing – original draft, Writing – review & editing. **Yaqin Wang:** Investigation, Data curation, Validation. **Kuan Chang:** Investigation. **Shuangli Yang:** Investigation. **Huijie Liu:** Methodology. **Qian Chen:** Data curation. **Zhaoxiong Xie:** Resources. **Qin Kuang:** Writing – original draft, Writing – review & editing, Supervision, Funding acquisition, Project administration.

Declaration of Competing Interest

The authors declare that they have no known competing financial interests or personal relationships that could have appeared to influence the work reported in this paper.

Data Availability

Data will be made available on request.

Acknowledgements

This work was supported by the National Key Research and Development Program of China (2017YFA0206801), and the National Natural Science Foundation of China (Nos. 22071202, 21931009, 21721001, and 21773190).

Declaration of Competing Interest

The authors report no declarations of interest.

Appendix A. Supporting information

Supplementary data associated with this article can be found in the online version at doi:10.1016/j.apcatb.2022.121961.

References

[1] G.A. Olah, Beyond oil and gas: the methanol economy, Angew. Chem. Int. Ed. Engl. 44 (2005) 2636–2639.
[2] P. Schwach, X. Pan, X. Bao, Direct conversion of methane to value-added chemicals over heterogeneous catalysts: challenges and prospects, Chem. Rev. 117 (2017) 8497–8520.
[3] Y. Liu, D. Deng, X. Bao, Catalysis for selected C1 chemistry, Chem 6 (2020) 2497–2514.
[4] Z. Jin, L. Wang, E. Zuidema, K. Mondal, M. Zhang, J. Zhang, C. Wang, X. Meng, H. Yang, C. Mesters, F.S. Xiao, Hydrophobic zeolite modification for in situ peroxide formation in methane oxidation to methanol, Science 367 (2020) 193–197.
[5] N. Agarwal, S.J. Freakley, R.U. McVicker, S.M. Althahban, N. Dimitratos, Q. He, D. J. Morgan, R.L. Jenkins, D.J. Willock, S.H. Taylor, C.J. Kiely, G.J. Hutchings, Aqueous Au-Pd colloids catalyze selective CH_4 oxidation to CH_3OH with O_2 under mild conditions, Science 358 (2017) 223–227.
[6] J. Shan, M. Li, L.F. Allard, S. Lee, M. Flytzani-Stephanopoulos, Mild oxidation of methane to methanol or acetic acid on supported isolated rhodium catalysts, Nature 551 (2017) 605–608.
[7] J. Zheng, J. Ye, M.A. Ortuno, J.L. Fulton, O.Y. Gutierrez, D.M. Camaioni, R. K. Motkuri, Z. Li, T.E. Webber, B.L. Mehdi, N.D. Browning, R.L. Penn, O.K. Farha, J. T. Hupp, D.G. Truhlar, C.J. Cramer, J.A. Lercher, Selective methane oxidation to methanol on Cu-Oxo dimers stabilized by zirconia nodes of an NU-1000 metal-organic framework, J. Am. Chem. Soc. 141 (2019) 9292–9304.
[8] G.J. Hutchings, Methane activation by selective oxidation, Top. Catal. 59 (2016) 658–662.
[9] G. Qi, T.E. Davies, A. Nasrallah, M.A. Sainna, A.G.R. Howe, R.J. Lewis, M. Quesne, C.R.A. Catlow, D.J. Willock, Q. He, D. Bethell, M.J. Howard, B.A. Murrer, B. Harrison, C.J. Kiely, X. Zhao, F. Deng, J. Xu, G.J. Hutchings, Au-ZSM-5 catalyses the selective oxidation of CH_4 to CH_3OH and CH_3COOH using O_2, Nat. Catal. 5 (2022) 45–54.
[10] S. Grundner, M.A. Markovits, G. Li, M. Tromp, E.A. Pidko, E.J. Hensen, A. Jentys, M. Sanchez-Sanchez, J.A. Lercher, Single-site trinuclear copper oxygen clusters in mordenite for selective conversion of methane to methanol, Nat. Commun. 6 (2015) 7546.
[11] S. Natesakhawat, J.W. Lekse, J.P. Baltrus, P.R. Ohodnicki, B.H. Howard, X. Deng, C. Matranga, Active sites and structure–activity relationships of copper-based catalysts for carbon dioxide hydrogenation to methanol, ACS Catal. 2 (2012) 1667–1676.
[12] A.J. Knorpp, A.B. Pinar, C. Baerlocher, L.B. McCusker, N. Casati, M.A. Newton, S. Checchia, J. Meyet, D. Palagin, J.A. Bokhoven, Paired copper monomers in zeolite omega: the active site for methane-to-methanol conversion, Angew. Chem. Int. Ed. Engl. 60 (2021) 5854–5858.
[13] M. Ravi, M. Ranocchiari, J.A. van Bokhoven, The direct catalytic oxidation of methane to methanol–a critical assessment, Angew. Chem. Int. Ed. Engl. 56 (2017) 16464–16483.
[14] H. Zhou, Z. Chen, A.V. López, E.D. López, E. Lam, A. Tsoukalou, E. Willinger, D. A. Kuznetsov, D. Mance, A. Kierzkowska, F. Donat, P.M. Abdala, A. Comas-Vives, C. Copéret, A. Fedorov, C.R. Müller, Engineering the Cu/Mo_2CT_x (MXene) interface to drive CO_2 hydrogenation to methanol, Nat. Catal. 4 (2021) 860–871.
[15] H. Song, X. Meng, Z.-j. Wang, H. Liu, J. Ye, Solar-energy-mediated methane conversion, Joule 3 (2019) 1606–1636.
[16] H. Song, X. Meng, S. Wang, W. Zhou, X. Wang, T. Kako, J. Ye, Direct and selective photocatalytic oxidation of CH_4 to oxygenates with O_2 on cocatalysts/ZnO at room temperature in water, J. Am. Chem. Soc. 141 (2019) 20507–20515.
[17] Y. Zhou, L. Zhang, W. Wang, Direct functionalization of methane into ethanol over copper modified polymeric carbon nitride via photocatalysis, Nat. Commun. 10 (2019) 506.
[18] X. Chen, Y. Li, X. Pan, D. Cortie, X. Huang, Z. Yi, Photocatalytic oxidation of methane over silver decorated zinc oxide nanocatalysts, Nat. Commun. 7 (2016) 12273.
[19] Q. Li, Y. Ouyang, H. Li, L. Wang, J. Zeng, Photocatalytic conversion of methane: recent advancements and prospects, Angew. Chem. Int. Ed. Engl. 61 (2021), e202108069.
[20] M.S.A. Sher Shah, C. Oh, H. Park, Y.J. Hwang, M. Ma, J.H. Park, Catalytic oxidation of methane to oxygenated products: recent advancements and prospects for electrocatalytic and photocatalytic conversion at low temperatures, Adv. Sci. 7 (2020), 2001946.
[21] F. Sastre, V. Fornes, A. Corma, H. Garcia, Selective, room-temperature transformation of methane to C1 oxygenates by deep UV photolysis over zeolites, J. Am. Chem. Soc. 133 (2011) 17257–17261.
[22] J. Xie, R. Jin, A. Li, Y. Bi, Q. Ruan, Y. Deng, Y. Zhang, S. Yao, G. Sankar, D. Ma, J. Tang, Highly selective oxidation of methane to methanol at ambient conditions by titanium dioxide-supported iron species, Nat. Catal. 1 (2018) 889–896.
[23] X. Yu, V. De Waele, A. Lofberg, V. Ordomsky, A.Y. Khodakov, Selective photocatalytic conversion of methane into carbon monoxide over zinc-heteropolyacid-titania nanocomposites, Nat. Commun. 10 (2019) 700.
[24] Y. Wang, J. Zhang, W.X. Shi, G.L. Zhuang, Q.P. Zhao, J. Ren, P. Zhang, H.Q. Yin, T. B. Lu, Z.M. Zhang, W single-atom catalyst for CH_4 photooxidation in water vapor, Adv. Mater. (2022), e2204448.
[25] H. Song, X. Meng, S. Wang, W. Zhou, S. Song, T. Kako, J. Ye, Selective photo-oxidation of methane to methanol with oxygen over dual-cocatalyst-modified titanium dioxide, ACS Catal. 10 (2020) 14318–14326.
[26] X. Wu, Q. Zhang, W. Li, B. Qiao, D. Ma, S.L. Wang, Atomic-scale Pd on 2D titania sheets for selective oxidation of methane to methanol, ACS Catal. 11 (2021) 14038–14046.
[27] L. Luo, Z. Gong, Y. Xu, J. Ma, H. Liu, J. Xing, J. Tang, Binary Au-Cu reaction sites decorated ZnO for selective methane oxidation to C1 oxygenates with Nearly 100 % selectivity at room temperature, J. Am. Chem. Soc. 144 (2021) 740–750.
[28] L. Luo, J. Luo, H. Li, F. Ren, Y. Zhang, A. Liu, W.X. Li, J. Zeng, Water enables mild oxidation of methane to methanol on gold single-atom catalysts, Nat. Commun. 12 (2021) 1218.
[29] X. Yu, V.L. Zholobenko, S. Moldovan, D. Hu, D. Wu, V.V. Ordomsky, A. Y. Khodakov, Stoichiometric methane conversion to ethane using photochemical looping at ambient temperature, Nat. Energy 5 (2020) 511–519.
[30] S. Song, H. Song, L. Li, S. Wang, W. Chu, K. Peng, X. Meng, Q. Wang, B. Deng, Q. Liu, Z. Wang, Y. Weng, H. Hu, H. Lin, T. Kako, J. Ye, A selective $Au\text{-}ZnO/TiO_2$ hybrid photocatalyst for oxidative coupling of methane to ethane with dioxygen, Nat. Catal. 4 (2021) 1032–1042.
[31] N. Feng, H. Lin, H. Song, L. Yang, D. Tang, F. Deng, J. Ye, Efficient and selective photocatalytic CH_4 conversion to CH_3OH with O_2 by controlling overoxidation on TiO_2, Nat. Commun. 12 (2021) 4652.
[32] M. Xiao, Z. Wang, M. Lyu, B. Luo, S. Wang, G. Liu, H.M. Cheng, L. Wang, Hollow nanostructures for photocatalysis: advantages and challenges, Adv. Mater. 31 (2019), 1801369.
[33] P. Zhang, X.W.D. Lou, Design of heterostructured hollow photocatalysts for solar-to-chemical energy conversion, Adv. Mater. 31 (2019), 1900281.
[34] S.A. Ansari, M.M. Khan, M.O. Ansari, M.H. Cho, Nitrogen-doped titanium dioxide (N-doped TiO_2) for visible light photocatalysis, New J. Chem. 40 (2016) 3000–3009.
[35] X. Li, C. Wang, J. Tang, Methane transformation by photocatalysis, Nat. Rev. Mater. (2022), https://doi.org/10.1038/s41578-022-00422-3.
[36] Y. Fan, W. Zhou, X. Qiu, H. Li, Y. Jiang, Z. Sun, D. Han, L. Niu, Z. Tang, Selective photocatalytic oxidation of methane by quantum-sized bismuth vanadate, Nat. Sustain. 4 (2021) 509–515.
[37] S. Murcia-López, K. Villa, T. Andreu, J.R. Morante, Partial oxidation of methane to methanol using bismuth-based photocatalysts, ACS Catal. 4 (2014) 3013–3019.
[38] B. Sivaranjini, R. Mangaiyarkarasi, V. Ganesh, S. Umadevi, Vertical alignment of liquid crystals over a functionalized flexible substrate, Sci. Rep. 8 (2018) 8891.
[39] G.N. Nomikos, P. Panagiotopoulou, D.I. Kondarides, X.E. Verykios, Kinetic and mechanistic study of the photocatalytic reforming of methanol over Pt/TiO_2 catalyst, Appl. Catal. B 146 (2014) 249–257.